RESEARCH ARTICLE

Optoelectronic device based on lithium niobate nanofilms deposited at various pulsed laser wavelengths

Makram A. Fakhri[1] · Ali. A. Alwahib[1] · Sarmad Fawzi Hamza Alhasan[2] · Evan T. Salim[3] · Raed Khalid Ibrahim[4] · Forat H. Alsultany[5] · Ahmed W. Abdulwahab[1] · U. Hashim[6]

Abstract Lithium niobate is a promising material involved in a variety of optoelectronic device fabrication. In this paper, lithium niobate was prepared using the pulse laser deposition technique for designing a planer waveguide with enhanced properties. At different wavelengths of the pulsed laser, a nonphotonic lithium niobate thin film was deposited on the quartz substrate. Structural, optical, and electrical properties of the prepared films were studied and analyzed with X–ray diffraction and it found a single crystal peck location at $2\theta = 39.225°$ which corresponds to the phase of 006, scanning electron and atomic force microscopy, where the average size is found are ranged from 94 nm and the roughness are ranged from 8.5 to 11.3 nm, UV–VIS spectrophotometer, and electrical properties were investigated and found the deposited nanofilms have high transmissions are ranged 68–84%, and the energy bandgap values are 4.02 eV and 4.15 eV. A MOS device was created, and its electrical characteristics were well-supported.

Introduction

Lithium niobate becomes widely considered in the fabrication of various optoelectronic devices. Nowadays, industries are extensively integrating lithium niobate in their optical goods because of its remarkable optical and electrical properties [1–4].

Today's works of literature are rich in describing lithium niobate thin films in photonic applications such as optical modulators and waveguides because of their ferroelectric properties [5–7]. Comparing LiNbO$_3$ to any other bulk material, the literature showed that lithium niobate is more advantageous because of its ease of fabrication, the possibility of producing in a step-index manner, the possibility of dopant selectivity, and forming possibility in multilayer structure [8–11].

Due to its big and noticeable optical quality, LiNbO$_3$ is a good option for optical waveguide uses [12, 13]. The process of signal transfer with high quality source material for reduced loss is facilitated by the construction of optical waveguides using LiNbO$_3$ [14, 15]. The LiNbO$_3$ substance is one of the most extensively researched photonic crystals [16, 17]. Due to its high electro-optical coefficient and low optical losses, it is a very suitable material for optical communication systems, which are extensively used for uses in microwave telecommunications, optical switches, beam deflectors, memory units, and second harmonic generation [18–20].

The extraordinary linear and nonlinear optical characteristics, chemical stability, and mechanical robustness

✉ Makram A. Fakhri
mokaram_76@yahoo.com

✉ Evan T. Salim
evan_tarq@yahoo.com; evan.t.salim@uotechnology.edu.iq

1 Laser and Optoelectronic Department, University of Technology-Iraq, Baghdad, Iraq

2 Department of Communication Engineering, University of Technology-Iraq, Baghdad, Iraq

3 Department of Applied Science, University of Technology-Iraq, Baghdad, Iraq

4 AlFarahidi University, Baghdad, Iraq

5 Department of Medical Physics, Al-Mustaqbal University College, Hillah, Iraq

6 Institute of Nano Electronic Engineering, Universiti Malaysia Perlis, 01000 Kangar, Perlis, Malaysia

of LiNbO$_3$ make it an appealing host material for use in photonic crystal devices [21, 22]. The lattice constants for LiNbO$_3$'s hexagonal structure are $a = 0.5147$ nm and $c = 1.3862$ nm [23–25]. Additionally, LiNbO$_3$ has a lot of possible benefits from a business and technical perspective for integrated optics [26, 27]. Depending on the concentration of LiNbO$_3$, the straight and secondary energy bandgaps for LiNbO$_3$ are between (3.5–4.7 eV). Numerous variables, including flaws, makeup, and grain size, are blamed for these shifts [28–30].

Various techniques to prepare lithium niobate thin films are intensively outlined in the literature. Modified zoon melting, top-seeded solution growth, vertical Bridgman, and off-centered Czochralski growth are examples of deposition methods used to prepare LN thin films [31–33]. However, pulse laser deposition is a more superior and efficient technology used to prepare thin films. In PLD, a very short–high intensive laser pulse is used to evaporate the material surface. With particles escaping out of the material surface, they settled on the hosting substrate (e.g., quartz). This process should be performed inside a vacuum chamber to ensure the minimization of scattered particles and enhance the deposition purity of the samples [34–37].

The synthesis and physical analysis of mesoporous materials (MM), which have large surface areas and ordered groups of monodisperse pores with diameters variable between 2 and 50 nm, have advanced to an extraordinary level over the past two decades. This length measure has a certain element of "magic" to it because of the pertinent effects of surface proximity. Inorganic and organic materials, as well as nanospecies, have developed significant skills in the synthetic community for regulating the size and form of nanoscopic cavities. The success of MM as a vibrant and thriving essential area of study was facilitated by three benefits: (a) The capacity to precisely and independently regulate these materials' porosity, inorganic framework, and surface/pore contents, (b) the straightforward, prolonged reproducible, and affordable experimental procedures created by combining sol–gel approaches with self-assembly, and (c) the numerous sophisticated application options that take advantage of the confinement, chemical capabilities, and large surface area. While the initial focus was on using the large surface area in simple uses for catalysis, adsorption, or sensing processes, there is great potential in utilizing two less-used aspects: confinement effects because of the limited pore size and surface effects.[38–40]. Electrons are described in terms of their energy levels, potential wells, valence bands, conduction bands, and electron energy bandgaps by quantum confinement effects. When a particle's size is too small to be similar to the electron's wavelength, the quantum confinement effect is seen. It goes without saying that the material characteristics, specifically the Bohr radius aB, have a substantial impact on the containment of

an electron and hole in nanocrystals. These effects occur in larger nanocrystals and rely on the material's characteristics, specifically, on the Bohr radius, aB, which ranges between 2.34 nm and about 10 nm and contains Cd-related substances. As a general rule, the heavier the component atoms are, the smaller the bandgap of semiconductors becomes. When compared to a bulk semiconductor, nanoparticles with diameters of about 2 to 10 nm have a larger bandgap due to the quantum size effect, which causes different fluorescent hues to represent subtle variations in particle size [41, 42].

In this paper, the laser pulse deposition technique was used to prepare high-purity lithium niobate thin films for MOS devices and also for waveguiding applications using cheap, simple materials, also easy, and laboratory-available method process of preparing lithium niobite powder in addition to using the prepared powder to obtain a solid disk for the purpose of depositing the nanomaterial by the pulsed laser deposition method. At different wavelengths of the pulsed laser, samples will be deposited on a quartz substrate. To ensure good sample properties, all-optical and electrical properties of the prepared films will be deeply studied and examined using X–ray diffraction, scanning electron and atomic force microscopy, and UV–VIS spectrophotometer. A MOS device was created, and its electrical characteristics were well-supported.

Optical waveguides

One essential part of any photonic device is optical waveguides. Ensuring loss-less signal propagation within any photonic device has to be achieved by designing efficient optical waveguides [43, 44]. The primary function of an optical waveguide is to ensure high coupling efficiency between any sections of different refractive indices by modifying optical signal spot size to match the guiding requirements [8, 45]. Achieving low-loss optical signal at section interfaces and at the bending edges of the photonic devices enhances the ability to integrate devices in a single optical chip, and a more robust signal to confining disturbances [46–48].

Planar waveguide

Optical waveguides come in various geometric shapes. According to the applications, optical waveguides can be found in circular geometry (e.g., optical fibers), and planar waveguides [49, 50]. Planar waveguides facilitate the fabrication of various optical components at a single substrate to enhance device characteristics [51]. Examples of optical technologies with planer waveguides are beam splitters, attenuators, wavelength multiplexers, and optical modulators [52–54].

Good confining characteristics are satisfied by critically adjusting parameters to design optical waveguides [55, 56]. The refractive index is the most important parameter in achieving total guiding modes within the waveguide [57–59]. The fundamental property of any planar waveguide is the total number of modes as a function of layer thickness confined within the plane structure and the layer refractive index [60, 61]. Therefore, with a suitable and careful design of an optical waveguide, the total signal loss can be reduced to a negligible level. Such beneficial characteristics that optical technologies offer can reduce the gap of the future using integrated optics and integrated optoelectronic devices in the field of optical communication technology [51, 62, 63].

Experimental procedure

The experimental procedure used to prepare lithium niobate thin film has been illustrated in this section. The main materials used in this study are ultra-pure $Nb2_2O_5$, Li_2CO_3, and ethanol solution. At a molar ratio of 2.5:2.5, Li_2CO_3 and Nb_2O_5 are firstly mixed and then dissolved in 15 ml of ethanol solution. The purpose of dissolving the mixture in ethanol is to maximize the formation of the $LiNbO_3$ stoichiometry phase. This process has been performed with continuous heating and stirring at 500°C for 4 hours. A drying process was taken to get lithium niobate powder as a second step. To ensure organic removal, the powder is heated to 1000°C for 4 hours in static air under an oxygen atmosphere. As a further step, the powder is then collected, compressed under 20 tons in a pressing machine, and then fabricated as circular slaps of (1cm × 0.5cm) dimension.

Figure 1 shows the fabrication process of lithium niobate thin films on a quartz substrate using a pulsed laser deposition technique. The parameters used during the deposition process are listed in Table 1. An X–ray Pert Pro MRD PW3040 diffractometer (HR–XRD) device was used to evaluate the characteristics of the samples. This system is equipped with Cu–K alpha radiation of 0.15148 nm wavelength. More evaluation analyses were used by examining sample thickness using Filmetrics F20 scanning optical reflectometer. Investigation of the prepared sample's morphological properties, surface roughness, and optical properties was examined using JOEL JSM 6460LV scanning electron microscopy, SPM 9600 atomic force microscopy devices. The nanofilms thickness of the deposited nanostructures was tasted by the optical scanning reflectometer (Filmetrics, model: F20, from USA).

For optical results, firstly the optical characteristics of the deposited coatings are examined in the ultraviolet to near-IR range to determine their Transmission, Absorbance is tested using a spectrophotometer (double-beam UV–vis spectrophotometer of the (Shimadzu UV–VIS 1800, Japan)), then the optical reflection has been tested using the a reflectance UV–VIS diffuse spectrometer (Avantes model DH-S-BAL-24048 UV–VIS, from the Netherlands) device.

Fig. 1 Pulse laser deposition system
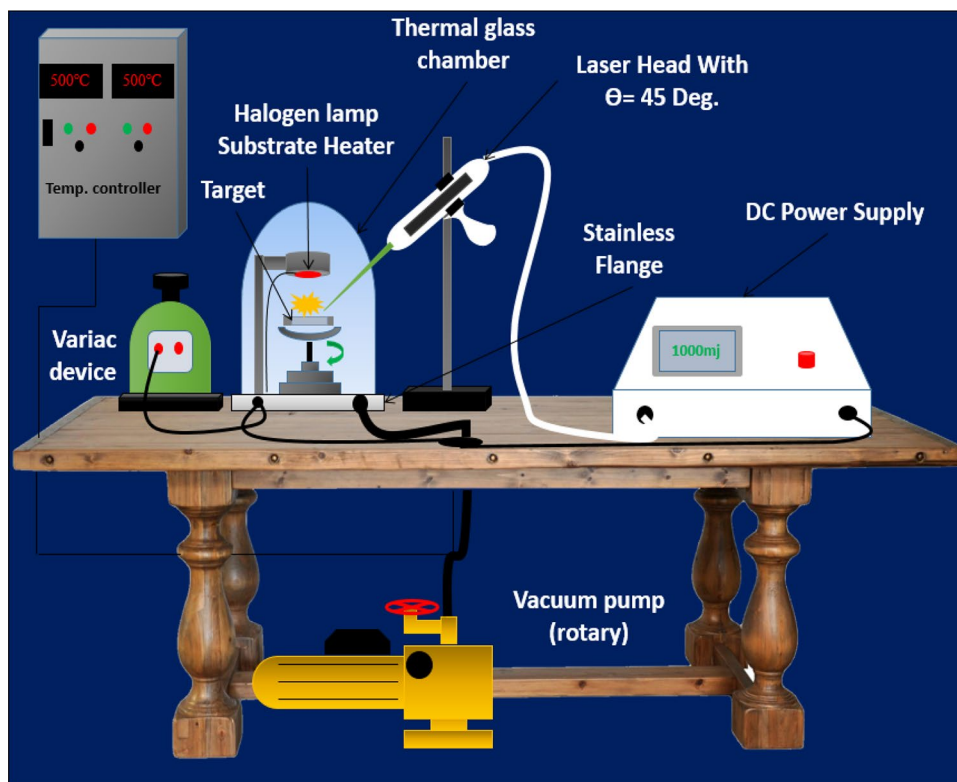
Table 1 The process conditions for deposition thin films

Parameters	Values	Parameters	Values
Laser fluence energy	2 J/cm^2	Angle of laser head with target	$\theta = 45°$
Laser shoots	200 pulses	Laser head to target distance	12 cm
Target to substrate distance	3 cm	Laser frequency	3 Hz
Vacuum pressure	10^{-2} mpar	Substrate temperature	500 °C
Laser pulse duration	6 ns	Laser wavelength	1064 nm 532 nm

Using Equation (1), the incident photon's energy was calculated [64–66].

$$Eg\,(eV) = 1.24/\,\lambda\,(\mu m) \tag{1}$$

where Eg is the bandgap energy and is the incident photon's frequency. The Tauc Equation 2 is used to determine the relationship between absorption coefficient and stimulation ratio [67, 68]:

$$(\alpha h\nu) = B\,(h\nu - Eg)r \tag{2}$$

where (α) is the absorption coefficient, (h) is the Planck constant, (ν) is the speed of light in the medium, (B) is a constant inversely proportional to the amorphousness, and (r) is a constant with a range of values depending on the type of substance.

Assuming that the phrase ($h\nu$)$1/r$ is equal to zero, we used to remember the optical bandgap energy value from the linear relationship (straight portion) between ($\alpha h\nu$)$1/r$ versus ($h\nu$). The wavelength's absorption coefficient is determined using equation (3) [69–71]:

$$\alpha = 2.303(A/t) \tag{3}$$

t is the thickness of the thin films, and A is the absorptance.

The value of the refractive index for the deposited nanofilms was calculated using a formula (4) [72–74].

$$n = n_s\left(\frac{1 + \sqrt{R}}{1 - \sqrt{R}}\right)^{1/2} \tag{4}$$

A MOS device was constructed employing (100nm) LN thin film as the dielectric layer after the best conditions were attained. Top and lower contacts made of aluminum. A constructed device's electrical characteristics were evaluated.

Results and discussion

Film thicknesses

The variation in the deposited sample's thickness was tested using an optical reflectometer device. A clear decrease in the thickness values using the second harmonic generation (532 nm), where its thickness is around 700 nm, while the thickness of the nanofilm that was deposited using the wavelength of 1064 nm is approximately 1 µm. This reduction indicates a good correlation with the positive modifications on the size of the grain that guide to the enhancement of the surface to become smoother.

Structural properties

The thin films prepared under high annealing temperature of 500°C showed a development at their crystalline structure. For such result, the using of lithium niobate thin films as a waveguide become possible. The X-ray diffractometer showed peak locations at $2\theta = 39.225°$. This peak corresponds to the material phases of 006 as shown in Fig. 2, which indicates single crystal phase samples. These results matching with the previously presented results [75, 76].

Surface morphology properties

Figure 3 presents the SEM results of the samples that were deposited at two different wavelengths, where it seems clear that the surface becomes smoother and more homogeneous as a result of the deposition process by changing the wavelength from 1064 to 532 nm, and this improvement was due to the effect of laser energy on the extraction and ablation process. It is clear that the deposition process improved the grain sizes and their distribution in the lower wavelength (using the second harmonic generation), where it was found that the average grain size when using the second harmonic generation of the pulsed laser is 94 nm, these results are identical to the results presented previously [77, 78].

The characteristics of the samples that were deposited at different wavelengths also show that there is a significant improvement in the surface roughness at the optimal wavelength for pulsed laser (using the second harmonic generation of the pulsed laser), where it observed that the surface roughness increases with the use of the second harmonic generation, ranging from 11.3 nm for a 532 nm pulsed laser to 8.5 nm for a 1064 nm pulsed laser, these results are recorded by AFM as shown in Fig. 4, Where the figure presents the results of the deposited films in the case of two dimensions and in the case of three dimensions.
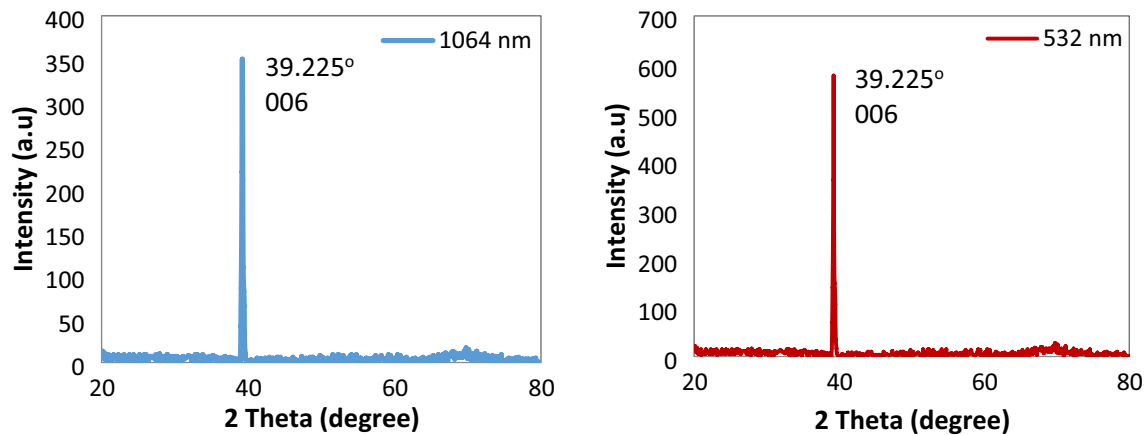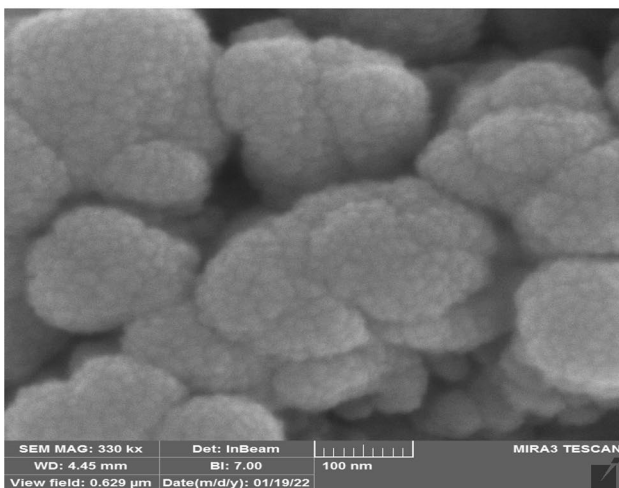
Fig. 2 XRD patterns of LiNbO$_3$ thin film prepared with PLD on quartz substrate at different wavelengths and thickness of 700 nm at 532 nm, 1000 nm at 1064 nm
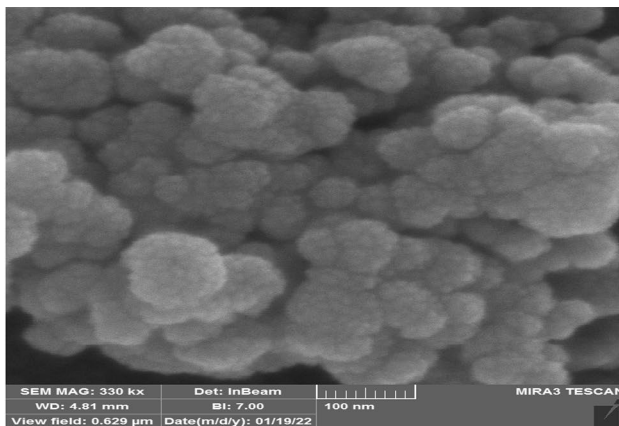
532 nm

1064 nm

Fig. 3 SEM images of LiNbO$_3$ thin film prepared on quartz substrate at different wavelengths and thickness of 700 nm at 532 nm, 1000 nm at 1064 nm

In both cases, the regulation of distribution and roughness appears clearly at its best when using the second harmonic generation in the deposition process. The reason is also due to the doubling of the sedimentation energy and removal process of the nanoparticles, and due to the restructuring and re-arrangement in the crystals that improved the structural properties, these results are in agreement with the results presented previously [79, 80].

Optical properties

At wavelength ranges from 200 to 1000 nm, the ultraviolet–visible technique was used to examine the transmission parameters of the prepared samples. Figure 5a shows the transmission values of two wavelengths as a function of wavelength. The average transmittance value was 70% with white to brown colors of samples prepared at 500°C. Higher values of transmittance are attributed to the surface roughness enhancement (low roughness) as the annealing temperature goes high.

At wavelength ranges from 200 to 1000 nm, the ultraviolet–visible technique was used to examine the transmission parameters of the prepared samples. Figure 5a shows the transmission values of two wavelengths as a function of wavelength. The average transmittance value was 70% with white to brown colors of samples prepared at the pulsed laser wavelength of are1064 nm. Higher values of transmittance (83%) are attributed to the surface roughness enhancement (low roughness) as the wavelength of the pulsed laser goes down (532 nm) as a result of an increase in the pulsed laser energy.

Figure 5b presents the absorption spectra as a function of wavelength ranges. Despite the sharp absorption at about 300nm which results due from the micro- and nano-confinement effect of the lithium niobate, the total curve showed
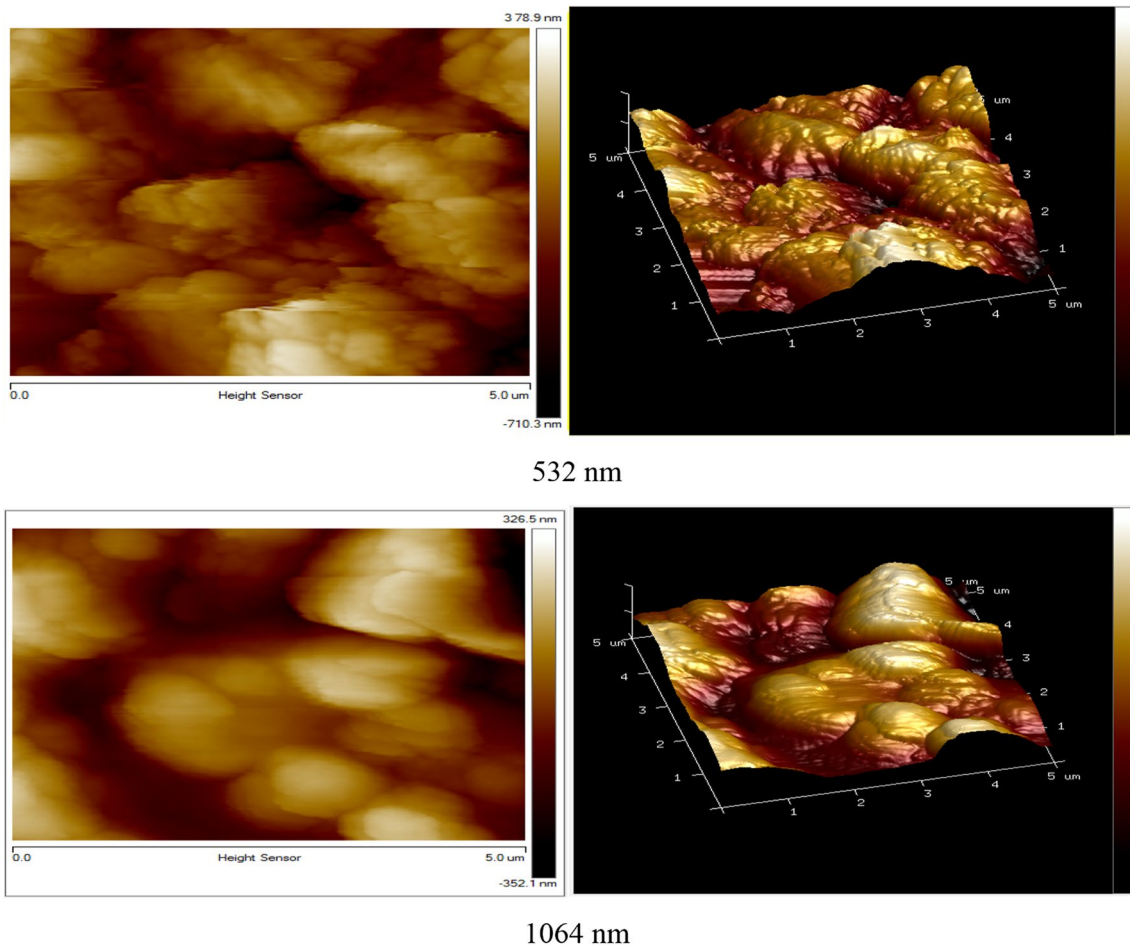
532 nm

1064 nm

Fig. 4 2D and 3D AFM images of LiNbO$_3$ thin film prepared on quartz substrate at different wavelengths and thickness of 700 nm at 532 nm, 1000 nm at 1064 nm

very weak absorption values at UV–VIS region as a result of porosity existence. These results match with the previously presented results [81, 82].

According to the reflectance spectra, Fig. 6a shows the reflectance as a function of wavelength. The values are shown to increase as the wavelength increases and ranged from 20 to 35 % of the reflectively were recorded at the visible and IR region of the spectrum. Further, a steady change in the values of the refractive index at the visible and infrared spectrum is presented in Fig. 6b. The refractive index values are calculated from reflectance values obtained in Fig. 6a and graphed as a function of wavelength. At the visible region, the value of the refractive index was found to be 2.45 at 273nm, which is considered a very high value suitable for waveguide applications. These results matching with the previously presented results [83, 84].

Figure 7 presents the energy bandgap values of the prepared thin films at different wavelengths. Two curves were drawn referring to two wavelengths; 532 nm and 1064 nm. The curve has been estimated by plotting $(\alpha h v)^2$ as a function of the photon energy (hv). It was found that the energy

bandgap values are 4.02 eV and 4.15 eV, which they are relatively large compared to any bulk materials, where this difference in values is due to the difference in the granular size of the nanostructures that have been deposited and as a result of the different wavelengths, and thus the effect of the energy of each wave and its effect on the particle size, roughness, and structural and optical results appeared. These results match the previously presented results [51, 85, 86].

By measuring the I-V characteristics of the prepared samples at various pulsed laser wavelengths, it is possible to examine the electrical properties. The I-V characteristics of the produced samples are displayed in Fig. 8a and b under both dark and light settings by using a lamp of halogen with power intensity of 100 mW/cm^2 at the room temperature. Maximum current ensures the establishment of the depletion zone to execute electron–hole pairs associated to every incident photon under lighting conditions. The transmittance value of the films becomes more sensitive to the UV–NIR spectrum range with a high chance of photon absorption creating electron–hole pair, leading to strong photocurrent capacity, as the annealing temperature rises. However, at the
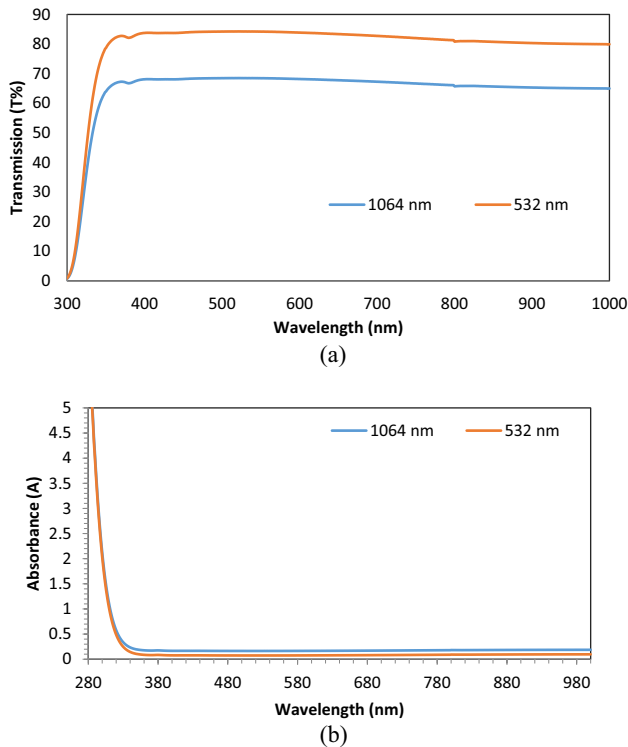
Fig.5 a Transmission spectra and **b** the absorbance film spectra of the LiNbO$_3$ nanostructures deposited at different wavelengths and thickness of 700 nm at 532 nm, 1000 nm at 1064 nm

optimum pulsed laser wavelength (532 nm) in both dark and light circumstances, the greatest increase in the current value of the produced samples was seen. With the created thin film's excellent electrical qualities, it may be used for optical waveguide applications by supplying an external voltage source to assure light propagation inside the device, as shown in the reference's illustrations [87, 88]. Figure. 8 a, b shows the I-V characteristic of a manufactured MOS device in a dark environment for a device that has been constructed at the ideal pulsed laser wavelength; the obtained findings demonstrate satisfactory rectification. Figure 8b illustrates electrical current under illumination. The increase in electrical current with incident light power is very obvious because an increase in incident photons per unit area leads to an increase in the generation of electron–hole pairs, which in turn increases the generation of net photocurrent density.

Conclusion

In this paper, a lithium niobate thin film was prepared, studied, and analyzed using pulse laser deposition technique for optical waveguide applications. The results showed that the nanostructure of the prepared samples are crystalline, smooth and in regular distribution in its structure with a single peak $2\theta = 39.225°$ corresponds
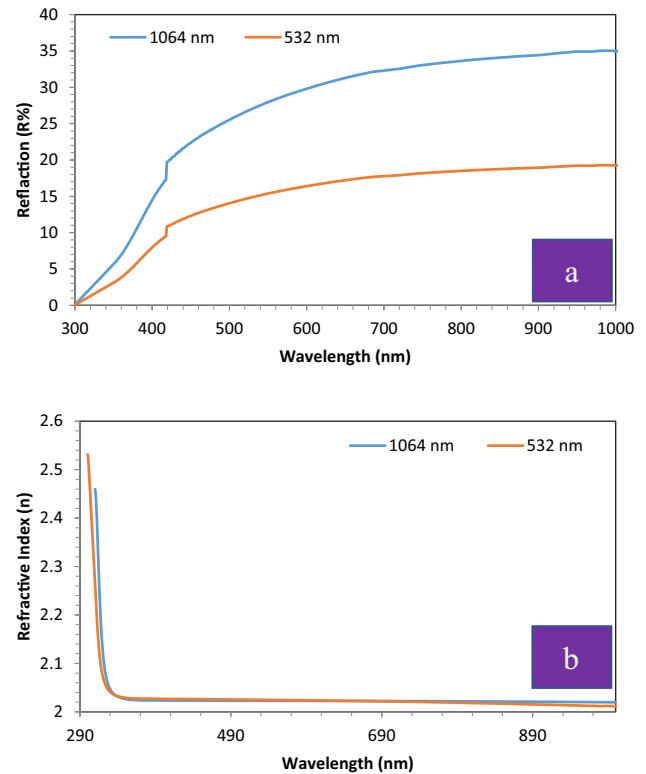

Fig. 6 a Reflectivity and **b** the refractive index of LiNbO$_3$ nanostructure as a function of wavelength with error ration of $\geq 10\%$ and thickness of 700 nm at 532 nm, 1000 nm at 1064 nm
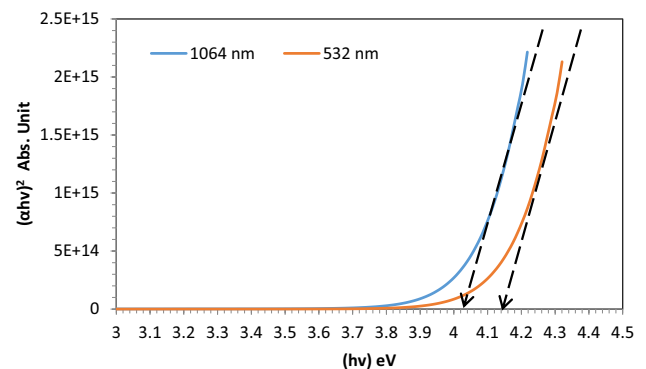
Fig. 7 Optical bandgap of LiNbO$_3$ nanostructure as a function of wavelength and thickness of 700 nm at 532 nm, 1000 nm at 1064 nm

to the phase location 006. High transmission, reflectance, and absorption values at the visible region of the spectrum indicate that the overall samples are suitable for waveguide applications. Since a successful rectification MOS device was created, lithium niobate may be used widely in optoelectronics applications due to its considerable features.
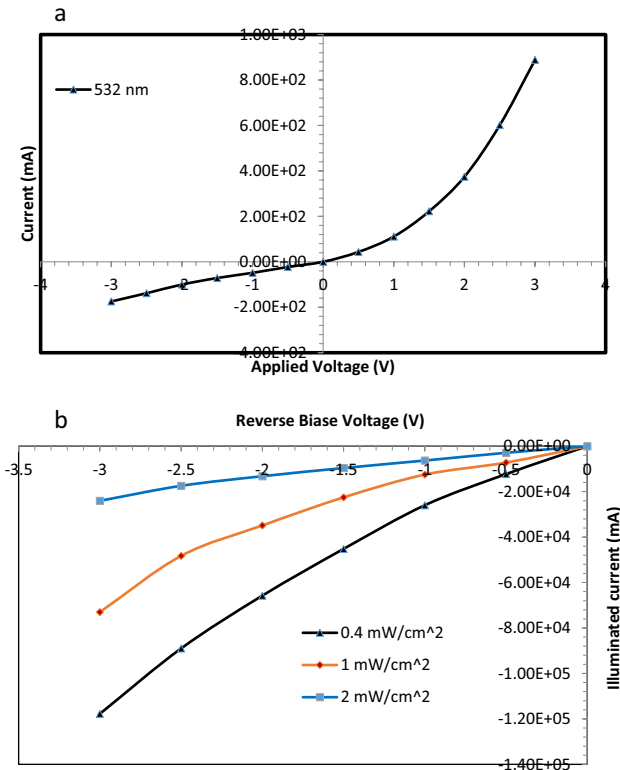
Fig. 8 I–V behavior LiNbO$_3$ thin films at **a** in dark, **b** under light effect at different incident power and thickness of 700 nm at 532 nm, 1000 nm at 1064 nm

References

1. M.A. Fakhri, E.T. Salim, A.W. Abdulwahhab, U. Hashim, M.A. Minshid, Z.T. Salim, 1. The effect of annealing temperature on optical and photolumence properties of LiNbO$_3$ Surf. Rev. Lett. **26**(10), 1950068 (2019)

2. D. Dai, Y. Tang, J.E. Bowers, Mode conversion in tapered submicron silicon ridge optical waveguides, Opt. Exp. **20**, 13425–13439 (2012)

3. L. Chen, Q. Xu, M.G. Wood, R.M. Reano, Hybrid silicon and lithium niobate electro-optical ring modulator. Optica **1**, 112–118 (2014)

4. M.A. Fakhri, N.H. Numan, M.H. Kheder, B.A. Badr, F.G. Khalid, U. Hashim, E.T. Salim, Z.T. Salim, Epitaxial growth of photonic LiNbO$_3$ nano crystals and structural studies using for waveguides. AIP Conf. Proc. **2045**, 020019 (2018)

5. X. Xu, Y.Q. Cao, P. Lu, J. Xu, W. Li, K.J. Chen, Electroluminescence devices based on Si quantum dots/SiC multilayers embedded in PN junction. IEEE Photon. J. **6**(1), 2200207–2200213 (2014)

6. J.-W. Son, S.S. Orlov, B. Phillips, L. Hesselink, Pulsed laser deposition of single phase LiNbO$_3$ thin film waveguides. J Electroceram **17**, 591–595 (2006)

7. M.A. Fakhri, N.H. Numan, Z.S. Alshakhli, M.A. Dawood, A.W. Abdulwahhab, F.G. Khalid, U. Hashim, E.T. Salim, Physical investigations of nano and micro lithium-niobate deposited by spray pyrolysis technique. AIP Conf. Proc. **2045**, 020015 (2018)

8. X. Wang, Z. Ye, G. Wu, L. Cao, B. Zhao, Growth of textured LiNbO$_3$ thin film on Si (111) substrate by pulsed laser deposition. Mater. Lett. **59**, 2994–2997 (2005)

9. X. Wang, Y. Liang, S. Tian, W. Man, J. Jia, Oxygen pressure dependent growth of pulsed laser deposited LiNbO$_3$ films on diamond for surface acoustic wave device application. J. Cryst. Growth **375**, 73–77 (2013)

10. M.H. Mohsin, N.H. Numan, E.T. Salim, M.A. Fakhri, Physical properties of sic nanostructure for optoelectronics applications. J. Renew. Mater. **9**(9), 1519–1530 (2021)

11. Y. Zheng, J. Duan, Optical properties of the coupling interface for planar optical waveguides. Optic. Photon. J. **1**, 106–109 (2011)

12. Z.T. Salim, U. Hashim, M.KMd. Arshad, M.A. Fakhri, E.T. Salim, Zinc oxide flakes-corolla lobes like nano combined structure for SAW applications. Mater. Res. Bull. **86**, 215–219 (2017)

13. R.A. Ismail, B.G. Rasheed, E.T. Salm, M. Al-Hadethy, High transmittance–low resistivity cadmium oxide films grown by reactive pulsed laser deposition. J. Mater. Sci.: Mater. Electron. **18**(10), 1027–1030 (2007)

14. E.T. Salim, I.R. Agool, M.A. Muhsien, Construction of SnO$_2$/SiO$_2$/Si Heterojunction and its Lineup Using I-V and C-V Measurements,. Int. J. Mod. Phys. B **25**(29), 3863–3869 (2011)

15. M.A. Fakhri, E.T. Salim, U. Hashim, A.W. Abdulwahhab, Z.T. Salim, Annealing temperature effect on structural and morphological properties of nano photonic LiNbO$_3$. J. Mater. Sci.: Mater. Electron. **28**(22), 16728–16735 (2017)

16. E.T. Salim, Rapid thermal oxidation for silicon nanocrystal based solar cell. Int. J. Nanoelectron. Mater. **5**(2), 95–100 (2012)

17. I. Savatinova, S. Tonchev, E. Popov, E. Liarokapis, C. Raptis, Raman scattering of proton exchanged LiNbO$_3$ waveguides. J. Phys. D Appl. Phys. **25**(1), 106–112 (1992)

18. S.M. Taleb, M.A. Fakhri, S.A. Adnan, Substrate and annealing temperatures effects on the structural results of LiNbO$_3$ photonic films using PLD method. AIP Conf. Proc. **2213**(1), 020234 (2020)

19. S.M. Taleb, M.A. Fakhri, S.A. Adnanm, Optical investigations of nanophotonic LiNbO$_3$ films deposited by pulsed laser deposition method. Defect Diffus. Forum **398**, 16–22 (2020)

20. M.C. Maldonado-Orozco, M.T. Ochoa-Lara, J.E. Sosa-Márquez, S.F. Olive-Méndez, P. Pizá-Ruiz, J.J.C. Quintanar-Sierra, F. Espinosa-Magaña, Characterization of Mn-doped electrospun LiNbO$_3$ nanofibers by Raman spectroscopy. Mater. Charact. **127**, 209–213 (2017)

21. Y. Al-Douri, M.A. Fakhri, N. Badi, C.H. Voon, Effect of stirring time on the structural parameters of nanophotonic LiNbO$_3$ deposited by spin-coating technique. Optik **156**, 886–890 (2018)

22. M.A. Muhsien, E.T. Salim, I.R. Agool, Preparation and characterization of (Au/n-Sn/Si/Si/Al) MIS device for optoelectronic application. J. Opt. **756402**, 9 (2013)

23. E.T. Salim, M.S. Al-Wazny, M.A. Fakhri, Glancing angle reactive pulsed laser deposition (grpld) for Bi$_2$O$_3$/Si heterostructure. Mod. Phys. Lett. B **27**(16), 1350122 (2013)

24. S.M. Taleb, M.A. Fakhri, S.A. Adnan, Physical investigations of nanophotonic LiNbO$_3$ films for photonic applications. J. Ovonic Res. **15**(4), 261–269 (2019)

25. E.T. Salim, Optoelectronic properties of Fe$_2$O$_3$/Si heterojunction prepared by rapid thermal oxidation method. Indian J. Phys. **87**(4), 349–353 (2013)

26. M.A. Fakhri, E.T. Salim, M.H.A. Wahid, U. Hashim, Z.T. Salim, R.A. Ismail, Synthesis and characterization of nanostructured LiNbO$_3$ films with variation of stirring duration. J. Mater. Sci. Mater. Electron. **28**(16), 11813–11822 (2017)

27. E.T. Salim, M.A. Fakhri, H. Hassen, Metal oxide nanoparticles suspension for optoelectronic devises fabrication. Int. J. Nanoelectron. Mater. **6**(2), 121–128 (2013)

28. M.A. Fakhri, M.H.A. Wahid, S.M. Kadhim, B.A. Badr, E.T. Salim, U. Hashim, Z.T. Salim, The structure and optical properties of Lithium Niobate grown on quartz for photonics application. Eur. Phys. J. Conf. **162**, 01005 (2017)

29. M.A. Fakhri, M.H.A. Wahid, B.A. Badr, S.M. Kadhim, E.T. Salim, U. Hashim, Z.T. Salim, Enhancement of Lithium Niobate nanophotonic structures via spin-coating technique for optical waveguides application. Eur. Phys. J. Conf. **162**(7), 01004 (2017)

30. R. Mouras, M.D. Fontana, M. Mostefa, P. Bourson, Photorefractive properties probed by Raman spectroscopy in Fe-doped LiNbO$_3$. J. Opt. Soc. Am. B **23**(9), 1867–1871 (2006)

31. Y. Lu, P. Dekker, Growth and characterization of lithium niobate planar waveguides by liquid phase epitaxy. J. Cryst. Growth **311**, 1441–1445 (2009)

32. F.H. Alsultany, S.F.H. Alhasan, E.T. Salim, Seed layer-assisted chemical bath deposition of Cu2$_O$ nanoparticles on ITO-coated glass substrates with tunable morphology, crystallinity, and optical properties. J. Inorg. Organomet. Polym. **31**, 3749–3759 (2021)

33. M. Nyman, T.M. Anderson, P.P. Provencio, Comparison of aqueous and non-aqueous soft-chemical syntheses of lithium niobate and lithium tantalate powders. Cryst. Growth Des. **9**, 1036–1040 (2009)

34. B.K. Yun, Y.K. Park, M. Lee, N. Lee, W. Jo, S. Lee, J. Hoon Jung, Lead-free LiNbO$_3$ nanowire-based nanocomposite for piezoelectric power generation. Nanoscale Res. Lett. **9**, 4–10 (2014)

35. R.A. Ismail, E.T. Salim, H.T. Halbos, Preparation of Nb$_2$O$_5$ nanoflakes by hydrothermal route for photodetection applications: The role of deposition time. Optik **245**, 167778 (2021)

36. E. Marenna, C. Aruta, E. Fanelli, M. Barra, P. Pernice, A. Aronne, Sol–gel synthesis of nanocomposite materials based on lithium niobate nanocrystals dispersed in a silica glass matrix. J. Solid State Chem. **182**, 1229–1234 (2009)

37. Ch. Fan, B. Poumellec, M. Lancry, X. He, H. Zeng, Three-dimensional photo precipitation of oriented LiNbO$_3$-like crystals in silica-based glass with femtosecond laser irradiation. Opt. Lett. **37**, 2955–2957 (2012)

38. I. Ichinose, T. Kunitake, Wrapping and inclusion of organic molecules with ultrathin, amorphous metal oxide films. Chem. Rec. **2**(5), 339–351 (2002)

39. C.T. Kresge, M.E. Leonowicz, W.J. Roth, J.C. Vartuli, J.S. Beck, Ordered mesoporous molecular sieves synthesized by a liquid-crystal template mechanism. Nature **359**, 710–712 (1992)

40. Y. Tsuneo, S. Toshio, K. Kazuyuki, K. Chuzo, The preparation of Alkyltrimethylammonium–Kanemite complexes and their conversion to microporous materials. Bull. Chem. Soc. Jpn. **63**, 988–992 (1990)

41. J.S. Beck, J.C. Vartuli, W.J. Roth, M.E. Leonowicz, C.T. Kresge, K.D. Schmitt, C.T.W. Chu, D.H. Olson, E.W. Sheppard, S.B. McCullen, J.B. Higgins, J.L. Schlenker, A new family of mesoporous molecular sieves prepared with liquid crystal templates. J. Am. Chem. Soc. **114**(27), 10834–10843 (1992)

42. Oleg D. Neikov, Nikolay A. Yefimov, in Handbook of Non-Ferrous Metal Powders (Second Edition) Nanopowders, 2019 uantum Confinement Effects

43. E.T. Salim, R.A. Ismail, H.T. Halbos, Deposition geometry effect on structural, morphological and optical properties of Nb2O5 nanostructure prepared by hydrothermal technique. Appl. Phys. A **126**, 891 (2020)

44. M. Liu, D. Xue, S. Zhang, H. Zhu, J. Wang, K. Kitamura, Chemical synthesis of stoichiometric lithium niobate powders. Mater. Lett. **59**(8–9), 1095–1097 (2005)

45. N.S.L.S. Vasconcelos, J.S. Vasconcelos, V. Bouquet, S.M. Zanetti, E.R. Leite, E. Longo, L.E.B. Soledade, F.M. Pontes, M. Guilloux-Viry, A. Perrin, M.I. Bernardi, J.A. Varelaa, Epitaxial growth of LiNbO$_3$ thin films in a microwave oven. Thin Solid Films **436**, 213–219 (2003)

46. E.T. Salim, J.A. Saimon, M.K. Abood, M.A. Fakhri, Effect of silicon substrate type on Nb$_2$O$_5$/Si device performance: an answer depends on physical analysis. Opt. Quant. Electron. **52**(10), 463 (2020)

47. E.L. Wooten, K.M. Kissa, A. Yi-Yan, E.J. Murphy, D.A. Lafaw, P.F. Hallemeier, D. Maack, D.V. Attanasio, D.J. Fritz, G.J. McBrien, D.E. Bossi, A review of lithium niobate modulators for fiber-optic communications systems. IEEE J Sel. Topics Quantum Electron. **6**, 69–82 (2000)

48. T. Zhang, B. Wang, Y. Zhao, S. Fang, D. Ma, Y. Xu, Optical homogeneity and second harmonic generation in Li-rich Mg-doped LiNbO$_3$ crystals. Mater. Chem. Phys. **88**, 97–101 (2004)

49. E.T. Salim, J.A. Saimon, M.K. Abood, M.A. Fakhri, Electrical conductivity inversion for Nb$_2$O$_5$ nanostructure thin films at different temperatures. Mater. Res. Express **6**(12), 126459 (2019)

50. P. Galinetto, M. Marinone, D. Grando, G. Samoggia, F. Caccavale, A. Morbiato, M. Musolino, Micro-Raman analysis on LiNbO$_3$ substrates and surfaces: compositional homogeneity and effects of etching and polishing processes on structural properties. Opt. Lasers Eng. **45**, 380–384 (2007)

51. W. Kim, S. Kwon, W. Jeong, G. Son, K. Lee, W. Choi, W. Yang, H. Lee, H. Lee, Integrated optical modulator for signal up-conversion over radio-on-fiber link. Opt. Express **17**, 2638–2645 (2009)

52. M.K. Abood, M.H.A. Wahid, J.A. Saimon, E.T. Salim, Physical properties of Nb$_2$O$_5$ thin films prepared at 12M ammonium concentration. Int. J. Nanoelectron. Mater. **11**(Special issue BOND21), 237–244 (2018)

53. J. Guo, J. Zhu, W. Zhou, X. Huang, A plasmonic electro-optical variable optical attenuator based on side-coupled metal–dielectric–metal structure. Opt. Commun. **294**, 405–408 (2013)

54. D. Jannerl, D. Tulli, M. Garcıa-Granda, M. Belmonte, V. Pruneri, Micro structured integrated electro optic LiNbO$_3$ modulators. Laser Photo. Rev. **3**, 301–313 (2009)

55. M.A. Fakhri, A.W. Abdulwahhab, M.A. Dawood, A.Q. Raheema, N.H. Numan, F.G. Khalid, E.T. Salim, Optical investigations of nano lithium niobate deposited by spray pyrolysis technique with injection of Li$_2$CO$_3$ and Nb$_2$O$_5$ as raw materials. Int. J. Nanoelectron. Mater **11**(Special issue BOND21), 103–108 (2018)

56. M.R.R. Gesualdi, C. Jacinto, T. Catunda, M. Muramatsu, V. Pilla, Thermal lens spectrometry in pyroelectric lithium niobate crystals. Appl. Phys. B **93**, 879–883 (2008)

57. V. Ievlev, V. Shur, M. Sumets, A. Kostyuchenko, Electrical properties and local domain structure of LiNbO$_3$ thin film grown by

ion beam sputtering method. Acta Metall. Sinica (English Letters) **26**, 630–634 (2013)

58. A.A. Abdul-Hamead, F.M. Othman, M.A. Fakhri, Preparation of MgO–MnO$_2$ nanocomposite particles for cholesterol sensors. J. Mater. Sci.: Mater. Electron. **32**, 15523–15532 (2021)

59. P. Kumar, S.M. Babui, S. Perero, R.L. Sai, I. Bhaumik, S. Ganesamoorthy, A.K. Karnal, X-ray photoelectron spectroscopy, high-resolution X-ray diffraction and refractive index analyses of Ti-doped lithium niobate (Ti:LiNbO$_3$) nonlinear optical single crystal. Pramana J. Phys. **75**, 1035–1040 (2010)

60. N.E. Stankovaa, S.H. Tonchevb, E. Gyorgyc, G. Socolc, I. Mihailescuc, Pulsed laser deposition of LiNbO$_3$ thin films from Li-rich targets. J. Optoelectron. Adv. Mater. **6**, 1345–1348 (2014)

61. M.A. Fakhri, M.J. AbdulRazzaq, A.A. Alwahib, W.H. Muttlak, Theoretical study of a pure LinbO$_3$/Quartz waveguide coated gold nanorods using supercontinuum laser source. Opt. Mater. **109**, 110363 (2020)

62. Z. Zhou, B. Wang, Sh. Lin, Y. Li, K. Wang, Investigation of optical photorefractive properties of Zr:Fe:LiNbO$_3$ crystals. Opt. Laser Technol. **44**, 337–340 (2012)

63. P. Gangul, Semi-analytical analysis of lithium niobate photonic wires. Opt. Commun. **285**(21/22), 4347–4352 (2012)

64. B.K.H. Al-Maiyaly, I.H. Khudayer, A.J. Ibraheim, Effect ambient oxidation on structural and optical properties of copper oxide thin films. Eng. Technol. **3**, 8695–8700 (2014)

65. F. Idrees, C. Cao, F.K. Butt, M. Tahir, I. Shakir, M. Rizwan, Synthesis of novel hollow microflowers (NHMF) of Nb$_3$O$_7$F, their optical and hydrogen storage properties. Int. J. Hydrogen Energy **39**, 13174–13179 (2014)

66. F. Hattab, M. Fakhry, Optical and structure properties for nano titanium oxide thin film prepared by PLD. Engineering Sciences (FNCES), 2012 First National Conference, vol. 107, 1–5 (2012)

67. R. Das, S. Pandey, Comparison of optical properties of bulk and nano crystalline thin films of CdS using different precursors. Int. J. Mater. Sci. IJMS **1**, 35–40 (2011)

68. E.T. Salim, Surface morphology and x-ray diffraction analysis for silicon nanocrystal-based heterostructures. Surf. Rev. Lett. **20**(05), 1350046 (2013)

69. M.A. Fakhri, Y. Al-Douri, E.T. Salim, U. Hashim, Y. Yusof, E.B. Choo, Z.T. Salim, Y.N. Jurn, Structural properties and surface morphology analysia of nanophotonic LiNbO$_3$. ARPN J. Eng. Appl. Sci. **11**(8), 4974–4978 (2016)

70. A.S. Ibraheam, J.M. Rzaij, M.A. Fakhri, A.W. Abdulwahhab, Structural, optical and electrical investigations of Al:ZnO nanostructures as UV photodetector synthesized by spray pyrolysis technique. Mater. Res. Express **6**(5), 055916 (2019)

71. M.K. Abood, M.H.A. Wahid, E.T. Salim, J.A. Saimon, Niobium Pentoxide thin films employ simple colloidal suspension at low preparation temperature. EPJ Web of Conferences **162**, 01058 (2017)

72. D. Ciplys, R. Rimeika, I. Suarez, G. Lifante, M.S. Shur, A. Aulas, Guided-wave acousto-optic diffraction in Zn: LiNbO$_3$. Electron. Lett. **42**, 1294–1295 (2006)

73. Y. Al-Douri, M.A. Fakhri, A. Bouhemadou, R. Khenata, M. Ameri, Stirrer time effect on optical properties of nanophotonic LiNbO$_3$. Mater. Chem. Phys. **203**, 243–248 (2018)

74. V. Kumar, S.K. Sharma, T.P. Sharma, Band gap determination in thick films from reflectance measurements. Opt. Mater. **12**, 115–119 (1999)

75. H. Chen, T. Lv, A. Zheng, Y. Han, Discrete diffraction based on electro-optic effect in periodically poled lithium niobate. Opt. Commun. **294**, 202–207 (2013)

76. V. Ievlev, M. Sumets, A. Kostyuchenko, N. Bezryadin, Dielectric losses and ac conductivity of Si–LiNbO$_3$ heterostructures grown by the RF magnetron sputtering method. J. Mater. Sci.: Mater. Electron. **24**, 1651–1657 (2013)

77. Y. Kang, S. Jeong, S. Lee, J. Hwang, J. Kim, Hetero-epitaxial growth of LiNbO$_3$ thin film on GaN/Al$_2$O$_3$ by pulsed laser deposition. J. Korean Phys. Soc. **49**, 625–628 (2006)

78. B. Knabe, D. Schu Tze, T. Jungk, M. Svete, W. Ssenmacher, W. Mader, K. Buse, Synthesis and characterization of Fe-doped LiNbO$_3$ nanocrystals from a triple-alkoxide method. Phys. Status Solidi A. **208**, 857–862 (2011)

79. N. Ozer, C.M. Lampert, Electrochemical lithium insertion in sol-gel deposited Li/NbO$_3$ films. Sol. Energy Mater. Sol. Cells **39**, 367–375 (1995)

80. E.R. Camargo, M. Kakihana, Low temperature synthesis of lithium niobate powders based on water-soluble niobium malato complexes. Solid State Ionics **151**, 413–418 (2002)

81. K. Peithmann, M.R. Zamani-Meymian, M. Haaks, K. Maier, B. Andreas, K. Buse, H. Modrow, Fabrication of embedded waveguides in lithium-niobate crystals by radiation damage. Appl. Phys. B. **82**, 419–422 (2006)

82. R. Ageba, Y. Kadota, T. Maeda, N. Takiguchi, T. Morita, M. Ishikawa, Ultrasonically assisted hydrothermal method for ferroelectric material synthesis. J. Korean Phys. Soc. **57**, 918–923 (2010)

83. Y. Akiyama, K. Shitanaka, H. Murakami, Y. Shin, M. Yoshida, N. Imaishi, Epitaxial growth of lithium niobate film using metalorganic chemical vapor deposition. Thin Solid Films **515**, 4975–4979 (2007)

84. R. Grange, J.W. Choi, C.L. Hsieh, Y. Pu, A. Magrez, R. Smajda, L. Forró, D. Psaltis, Lithium niobate nanowires synthesis, optical properties, and manipulation. Appl. Phys. Lett. **95**, 143105–1431053 (2009)

85. H.K. Lam, J.Y. Dai, H.L.W. Chan, Orientation controllable deposition of LiNbO$_3$ films on sapphire and diamond substrates for surface acoustic wave device application. J. Cryst. Growth **268**, 144–148 (2004)

86. Y. Tan, F. Chen, M. Stepić, V. Shandarov, D. Kip, Reconfigurable optical channel waveguides in lithium niobate crystals produced by a combination of low-dose O3+ ion implantation and selective white light illumination. Opt. Express **16**, 10465–10470 (2008)

87. A.J. Waddie, A. Dzipalski, I. Thurston, M.R. Taghizadeh, Lithium Niobate (LiNbO$_3$) waveguides for electromagnetic pulse (EMP) sensing. IEEE Sen. J. **16**(14), 5603–5609 (2016)

88. M.M. Salih, Water pollution detection of tigris river by utilizing thermal remote sensing techniques: north Baghdad-Iraq region as a case study. Optica Pura y Aplicada **54**(1), 1–9 (2021)